



OPEN

Activin A plays an essential role in migration and proliferation of hepatic stellate cells via Smad3 and calcium signaling

Wei Zhang¹, Linjing Zhu², Fang Fang², Fenglin Zhang³, Runnan Wang², Ke Yang⁴, Yahui Liu^{1✉} & Xueling Cui^{2✉}

Activin A and hepatic stellate cells (HSCs) are involved in tissue repair and fibrosis in liver injury. This study investigated the impact of activin A on HSC activation and migration. A microfluidic D⁴-chip was used for examining the cell migration of mouse hepatic stellate cell line MHStc. The analysis of differentially expressed genes revealed that activin β A (*Inhba*), activin receptor type 1A (*Acvr1a*) and type 2A (*Acvr2a*) mRNAs were more significantly expressed in human HSCs than in the hepatocytes. Moreover, activin A promoted MHStc proliferation and induced MHStc migration. Furthermore, the MHStcs treated with activin A exhibited increased levels of migration-related proteins, N-cadherin, Vimentin, α -SMA, MMP2 and MMP9, but a decreased level of E-cadherin. Additionally, activin A treatment significantly increased the p-Smad3 levels and p-Smad3/Smad3 ratio in the MHStcs, and the Smad3 inhibitor SIS3 attenuated activin A-induced MHStc proliferation and migration. Simultaneously, activin A increased the calcium levels in the MHStcs, and the migratory effects of activin A on MHStcs were weakened by the intracellular calcium ion-chelating agent BAPTA-AM. These data indicate that activin A can promote MHStc activation and migration through the canonical Smad3 signaling and calcium signaling.

Keywords Hepatic stellate cells, Proliferation, Migration, Activin A, Smad3, Calcium signaling

The liver is composed of parenchymal cells (i.e., hepatocytes and cholangiocytes) as well as non-parenchymal cells (such as Kupffer cells [resident hepatic macrophages], liver sinusoidal endothelial cells [LSECs], and hepatic stellate cells [HSCs]). HSCs reside within the liver's space of Disse, and upon liver injury, these previously dormant HSCs undergo transformation in terms of both phenotype and metabolism, thereby adopting a myofibroblast (MFB)-like phenotype^{1,2}. As a response to liver injury, activated Kupffer cells and other mesenchymal cells produce and release numerous profibrotic cytokines, such as transforming growth factor β 1 (TGF β 1), platelet-derived growth factor (PDGF), and epidermal growth factor, thereby inducing HSC activation³⁻⁵. Activated HSCs (aHSCs) also produce a large amount of activin A⁶.

Activin A, a TGF- β superfamily member, is increasingly known for its involvement in various essential cellular processes, including the regulation of cell cycle progression and differentiation, apoptosis, metabolic and homeostatic control, tumorigenesis, and immune responses⁷⁻¹². Wound healing is also a well-established effect of activin A, and the dysregulation of this process causes pathological collagen accumulation and fibrosis. Activin A expression is notably augmented within cirrhotic and fibrotic liver tissues⁶. Carbon tetrachloride (CCl₄)-induced hepatic fibrosis can be mitigated by inhibiting activin A with its primary biological inhibitor, follistatin¹³. Stellate cells can migrate toward cytokine chemoattractants, thereby offering a partial explanation for their alignment within the inflammatory septa in vivo. Several chemoattractants, including PDGF, MCP-1, and CXCR3, have been identified to play a prominent role in this process¹⁴. Our prior study revealed that

¹Department of Hepatobiliary and Pancreatic Surgery, General Surgery Center, The First Hospital of Jilin University, Changchun 130021, Jilin, China. ²Department of Genetics, College of Basic Medical Sciences, Jilin University, Changchun 130021, Jilin, China. ³Department of Immunology, College of Basic Medical Sciences, Jilin University, Changchun 130021, Jilin, China. ⁴Institute of Applied Technology, Hefei Institutes of Physical Science, Chinese Academy of Sciences, Hefei 230031, Anhui, China. ✉email: yahui@jlu.edu.cn; cxl@jlu.edu.cn

activin A induces fibroblast migration as a novel chemokine¹⁵. However, whether activin A is involved in HSC migration remains unclear.

In this study, the mouse HSCs (MHStECs) were used to investigate the effects of activin A on HSC migration. We found that activin A promoted MHStEC proliferation and migration, but inhibited their adhesion, suggesting that activin A acts as a chemokine for HSC migration facilitating liver tissue remodeling during tissue repair and fibrosis. Activin A facilitates MHStEC activation and migration through calcium signaling, in addition to the canonical Smad-dependent pathway. These findings highlighted the potential role of activin A in HSCs as a novel therapeutic target for liver repair and fibrosis.

Results

Expression of activin A and its receptors in MHStECs

Differential gene expression analysis was performed between the freshly isolated mouse hepatocyte samples and 1-day-cultured HSC samples. To envisage the distribution of differentially expressed genes (DEGs) between the aforementioned samples, volcano plots were generated (Fig. 1A), in which the X-axis represents the fold change in gene expression and the Y-axis represents the statistical significance of the differences. According to the violin plot, the expression of activin β A (*Inhba*), activin receptor type 1A (*Acvr1a*) and *activin receptor type 2A* (*Acvr2a*) was markedly higher in HSCs than those in the hepatocytes, Kupffer cells, and LSECs (Fig. 1B). RT-PCR confirmed that the MHStECs expressed *Inhba*, *Acvr1a*, *Acvr2a*, *Acvr2b*, *Smad2*, and *Smad3* (Fig. 1C). Overall, these results indicate that MHStECs function both as producers of activin A and as its responsive cells.

Effect of activin A on the proliferation and wound healing of MHStECs

MHStEC proliferation was assessed using the cell counting kit-8 (CCK-8) assay and the real-time cell analysis (RTCA), which utilizes the principle of the microelectronic biosensor chip. RTCA enables label-free and continuous monitoring of cellular processes during experiments. Activin A was found to promote MHStEC proliferation in a dose-dependent manner (Fig. 2A), consistent with the results obtained using the RTCA (Fig. 2B). Hence, 10 ng/mL activin A was used for subsequent experiments. HSC proliferation is known to be linked to the liver tissue repair process following injury. Consequently, to investigate the impact of activin A on wound healing in MHStECs, wound scratch assays were conducted. The findings revealed that the group treated with 10 ng/mL activin A exhibited significantly enhanced wound healing compared with the control group treated with the culture medium alone (Fig. 2C).

Effect of activin A on MHStEC migration

The tissue repair process is influenced by the regenerative capacity of HSCs in wound healing as well as the phenomenon of cell migration. Hence, the effects of activin A on MHStEC migration were assessed through the transwell chamber and microfluidic cell migration assays. Activin A significantly increased the number of migrated MHStECs in the transwell chamber (Fig. 3A). However, cell migration is determined not only by the quantity of cells that migrate but also by the velocity and orientation of the movement of migrating cells. The microfluidic device can track the migration distance and trajectory of individual cells in real-time, thereby offering a more intuitive reflection of cell migration¹⁶. We here utilized the D⁴-chip of the microfluidic device to further evaluate the chemotactic migration of MHStECs toward activin A gradients. The results revealed that activin A elicited a higher number of migrated cells and facilitated a greater distance and stronger directionality of cell migration (Fig. 3B–F).

Effect of activin A on MHStEC adhesion

Changes in cell–cell adhesion generally initiate cell migration, and cell–substrate adhesion regulates the cell migration behaviors¹⁷. RTCA was first conducted to examine the effect of activin A on MHStEC adhesion. We noted that activin A significantly suppressed MHStEC adhesion in a dose-dependent manner (Fig. 4A). Moreover, the number of adhered cells was measured through the CCK-8 assay to evaluate the ability of cells to bind to the ECM. The number of MHStECs bound to the fibronectin-coated wells significantly decreased (Fig. 4B). ITGA5, as fibronectin is a major constituent of the ECM and plays a significant role in cell surface adhesion and signaling¹⁸. According to the differential gene expression analysis, the expression of *Itga5* was significantly higher in HSCs than in hepatocytes, Kupffer cells, and LSECs (Fig. 4C). Hence, the *Itga5* mRNA level in the adhered cells was determined through real-time quantitative RT-PCR, as evidenced by the activin A-induced downregulation of *Itga5* mRNA expression (Fig. 4D). These results were substantiated by the western blot analysis of ITGA5 protein expression (Fig. 4E). Collectively, these data provide direct evidence for the role of activin A in the inhibition of adhesion between MHStECs and ECM.

Effect of activin A on the expression of migration-related proteins and morphology of MHStECs

To confirm the regulatory role of activin A in cell migration, the expression of migration-related proteins in MHStECs was examined using western blotting. Activin A increased the levels of N-cadherin, Vimentin, α -SMA, and MMP9 proteins but decreased the levels of E-cadherin protein in MHStECs (Fig. 5A). Furthermore, Giemsa staining was used to determine the morphology of MHStECs. The activin A-treated groups exhibited enlarged cell bodies and larger protrusions (Fig. 5B), which suggested that activin A facilitates morphological changes in MHStECs, thereby conferring MHStECs with a MFB-like phenotype and the ability to migrate.

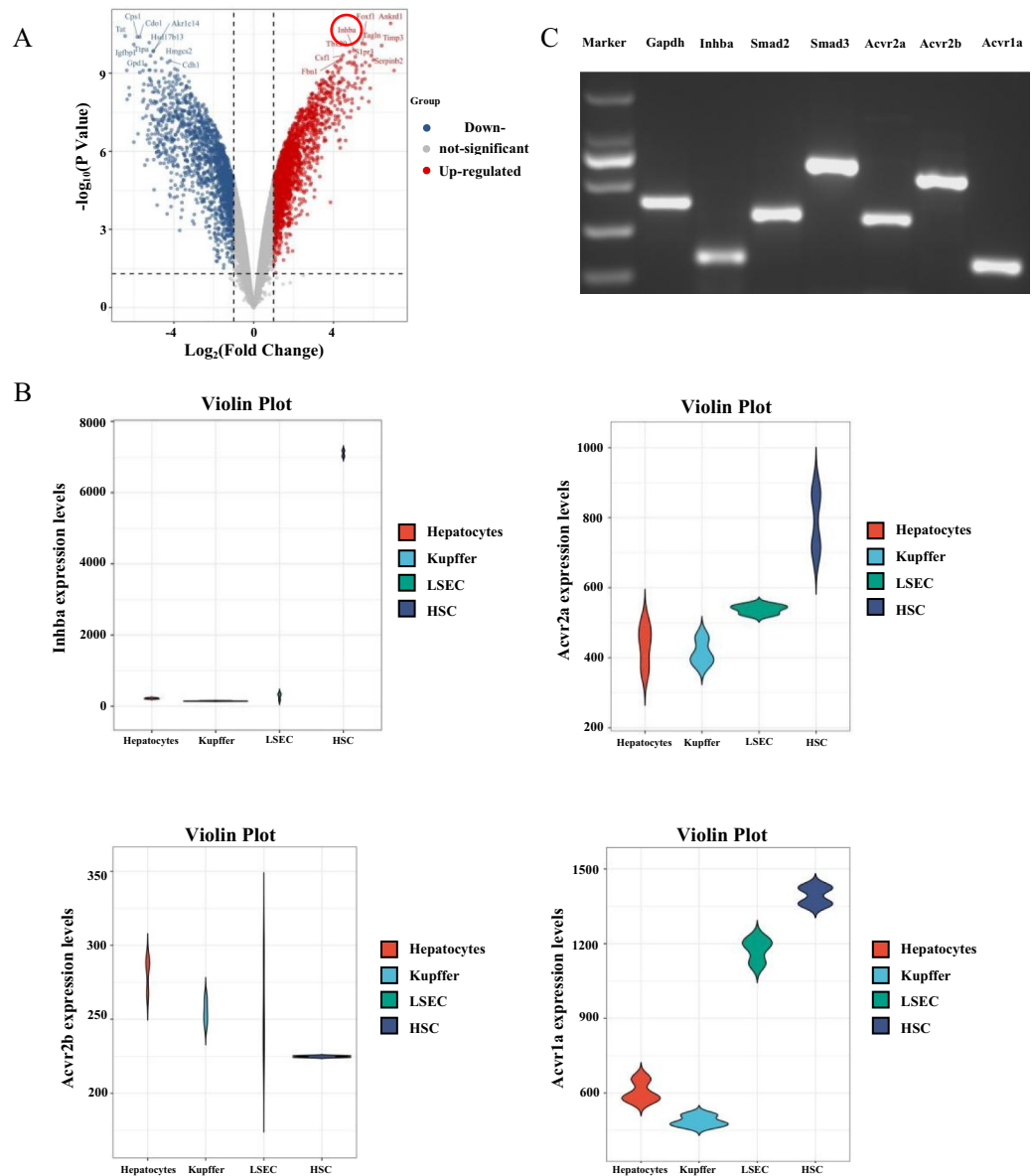


Fig. 1. Expression of activin A and its receptors in MHStCs. (A) The volcano plot illustrates the comparison of gene expression between the HSCs and hepatocytes. The x-axis represents the fold change in gene expression across various samples, while the y-axis represents the statistical significance of these differences. Significantly upregulated and downregulated genes were filtered ($|\log_2(\text{fold change})| > 1$, $\text{Padj} < 0.05$) and are highlighted using red and blue dots, respectively. Genes with no differential expression are depicted in gray. (B) The violin plots show *Inhba*, *Acvr2a*, *Acvr2b* and *Acvr1a* gene expression in hepatocytes, Kupffer cells, LSECs, and HSCs. (C) mRNA levels of *Gapdh*, *Inhba*, *Smad2*, *Smad3*, *Acvr2a*, *Acvr2b* and *Acvr1a* were measured using RT-PCR.

Effects of activin A on the expression of Smads and non-Smads signaling proteins in MHStCs

Activin A can initiate the canonical Smads signaling pathway and non-Smads signaling pathways. To determine the signal transduction mechanism through which activin A regulates MHStC migration, the levels of Smad3 and p-Smad3, Akt and p-Akt and JNK and p-JNK proteins were examined through western blotting. The results indicated a significant increase in the p-Smad3 protein level and p-Smad3/Smad3 ratio in the MHStCs following treatment with activin A, whereas no discernible alterations were observed in the levels of p-Akt and p-JNK, and the ratio of p-Akt/Akt and p-JNK/JNK ratio (Fig. 6A). Furthermore, pretreatment with the Smad3 inhibitor SIS3 significantly attenuated activin A-enhanced MHStC proliferation (Fig. 6B). Pretreatment with SIS3 also markedly downregulated activin A-induced MHStC migration (Fig. 6C). Altogether, these results indicate that activin A may enhance MHStC proliferation and migration through the canonical Smad3 signaling pathway, and not the non-canonical signaling pathway.

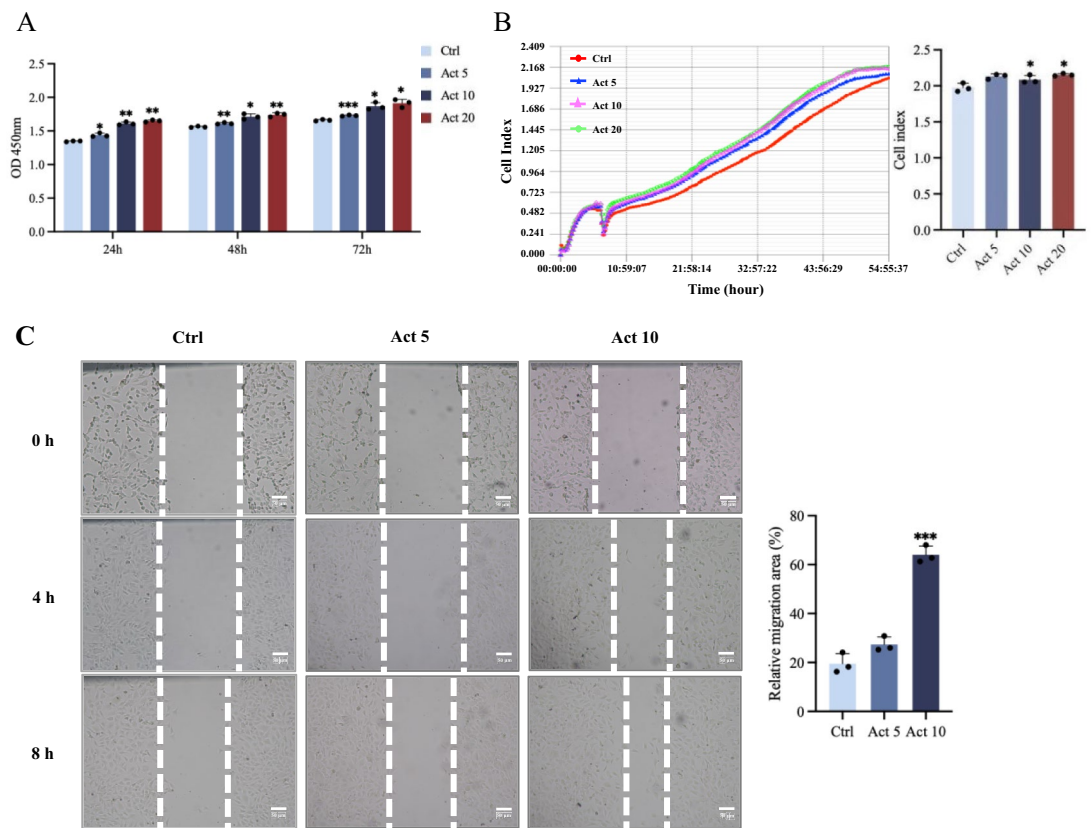


Fig. 2. Effect of activin A on MHStC proliferation and wound healing. **(A)** The CCK-8 assay was performed to assess the proliferation of MHStCs treated with different activin A concentrations for 24, 48, and 72 h. **(B)** Real-time MHStC proliferation was assessed through RTCA in 55 h. **(C)** The impact of activin A on wound healing in MHStCs was evaluated in wound scratch assays. The graph reflects the degree of wound healing from three separate experiments. Scale bar = 50 μ m. Ctrl, culture medium control. Act 5, 5 ng/mL activin A. Act 10, 10 ng/mL activin A. * $P < 0.05$, ** $P < 0.01$, *** $P < 0.001$ compared with the control group.

Effects of activin A on Ca^{2+} influx in MHStCs

A significant correlation has been reported between cell migration and intracellular calcium flow¹⁹. Activin A does not exert an impact on the intracellular calcium flux in breast cancer cells; however, it can enhance the intracellular calcium flux in fibroblasts^{14,16}. In the present study, activin A increased the influx of intracellular calcium in MHStCs (Fig. 7A). To confirm the potential involvement of calcium signaling in activin A-mediated cell migration, MHStCs were treated with the intracellular calcium ion-chelating agent BAPTA-AM, followed by the assessment of cell migration through the transwell assay. The results revealed that MHStC migration significantly increased in 10 ng/mL activin A diluted by 0.025% DMSO, compared with the control group treated with 0.025% DMSO alone. Furthermore, BAPTA-AM effectively attenuated the stimulatory effect of activin A on MHStC migration (Fig. 7B). Being a critical regulator of mitochondrial Ca^{2+} uptake, mitochondrial calcium uptake 1 (MICU1) facilitates oxidative metabolism and prevents the accumulation of mitochondrial calcium and subsequent cell death²⁰. A reduction in MICU1 levels results in excessive calcium accumulation within the mitochondria²¹. Therefore, we examined *Micu1* mRNA gene expression. Activin A treatment reduced *Micu1* mRNA expression (Fig. 7C). The aforementioned results suggested that activin A enhances calcium influx by inhibiting *Micu1* expression, consequently facilitating MHStC migration.

Discussion

In different forms of liver injury, such as infection, acute and chronic inflammatory responses, and the presence of other stimulating factors, HSCs can undergo proliferation and migrate toward local injured tissues, thereby contributing to tissue repair and remodeling. Due to liver injury, damaged cells in the liver microenvironment release ROS and pro-inflammatory cytokines, which, in turn, affect hepatocytes and HSCs^{22,23}. Additionally, excessive HSC activation and migration can result in the release of a large amount of cytokines and ECM, further contributing to liver tissue remodeling and fibrosis. The examination of the activation and migration mechanism of HSCs holds significance in facilitating liver repair and tissue remodeling. Activin A overexpression can elicit fibrotic responses in various organs, including the liver, lung, kidney, testicle, heart, conjunctiva, skin, and pancreas^{24–31}. Activin A promotes fibroblast proliferation in cases of chronic cardiac injury, resulting in tissue remodeling and exacerbating fibrosis within the cardiac tissue³². Studies have reported that hepatocytes, HSCs and LSECs are the main sources of activin A in the liver, and the expression profiles of type I and type II activin

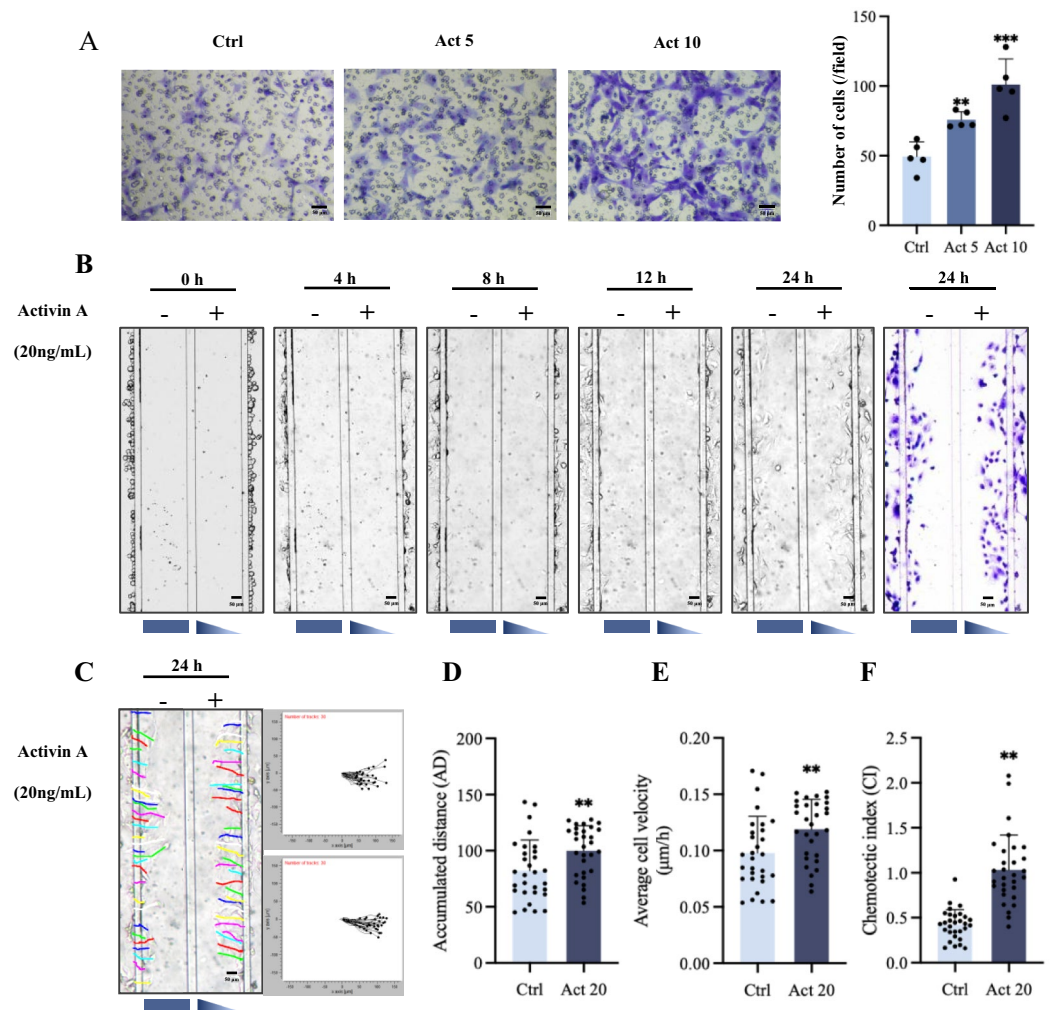


Fig. 3. Effect of activin A on MHStC migration. (A) MHStC migration in response to activin A (0–10 ng/mL) was analyzed through the transwell chamber assay. The cells that migrated through the porous membrane of the chamber were stained with Giemsa. (B–F) Effect of activin A on MHStC migration was assessed using the microfluidic device. Shown are the representative images of migrated cell distribution at 4 h, 8 h, 12 h and 24 h (B), trajectories of cell migration tracked for 24 h (C), accumulated migratory distance quantitated using Image J software (D), average cell migratory velocity (E), and chemotaxis index (CI) (F). Scale bar = 50 μm . Ctrl, culture medium control. Act 5, 5 ng/mL activin A. Act 10, 10 ng/mL activin A. Act 20, 20 ng/mL activin A. * $P < 0.05$, ** $P < 0.01$, *** $P < 0.001$ compared with the control group.

receptors differ across the liver cells^{6,33}. Furthermore, fibrosis induced by CCl_4 in the rat liver is concomitant with the increased activin A expression as well as HSC-induced activin A expression¹³. In this study, bioinformatic analysis indicated that the HSCs exhibited a significantly higher expression of activin βA than hepatocytes, KCs, and LSECs, and RT-PCR results showed that MHStCs expressed activin βA and activin receptors. These findings revealed that MHStCs could produce activin A as well as act as activin A-responsive cells.

After liver injury, HSCs become proliferative and contractile MFB-like cells, which have a quiescent phenotype in the healthy liver. HSC activation and proliferation have been identified as a critical event in hepatic injury development. In addition to the capacity for compensatory proliferation in response to hepatocyte damage, HSCs produce a large amount of ECM that surrounds the hepatocytes, thereby impeding their proliferation. Activin A can promote the proliferation and migration of various cells. For example, activin A promotes the proliferation of KPC (pancreatic ductal adenocarcinoma cell lines harboring $\text{Kras}^{\text{G12D}}$ and $\text{Trp53}^{\text{R172H}}$ mutations) through SMAD3 phosphorylation³⁴. Activin A secreted from the peripheral nerve fibroblasts can promote Schwann cell proliferation and migration³⁵. Moreover, activin A promotes cell proliferation, invasion, and migration, leading to a poor prognosis in patients with colorectal cancer³⁶. Herein, CCK8 and RTCA assays were conducted to explore the effect of activin A on MHStC proliferation. Activin A was found to dose-dependently promoted MHStC proliferation.

HSC activation, a crucial event in liver repair and fibrosis, is considered a key event in the epithelial–mesenchymal transition (EMT) process³⁷. The EMT process involves the reversible loss of polarity and change in the phenotype of epithelial cells to a mesenchymal fate. This conserved process is characterized by the disruption of cell–cell adhesions, enhanced migratory capabilities, and increased invasiveness. Activin A/activin-like kinase

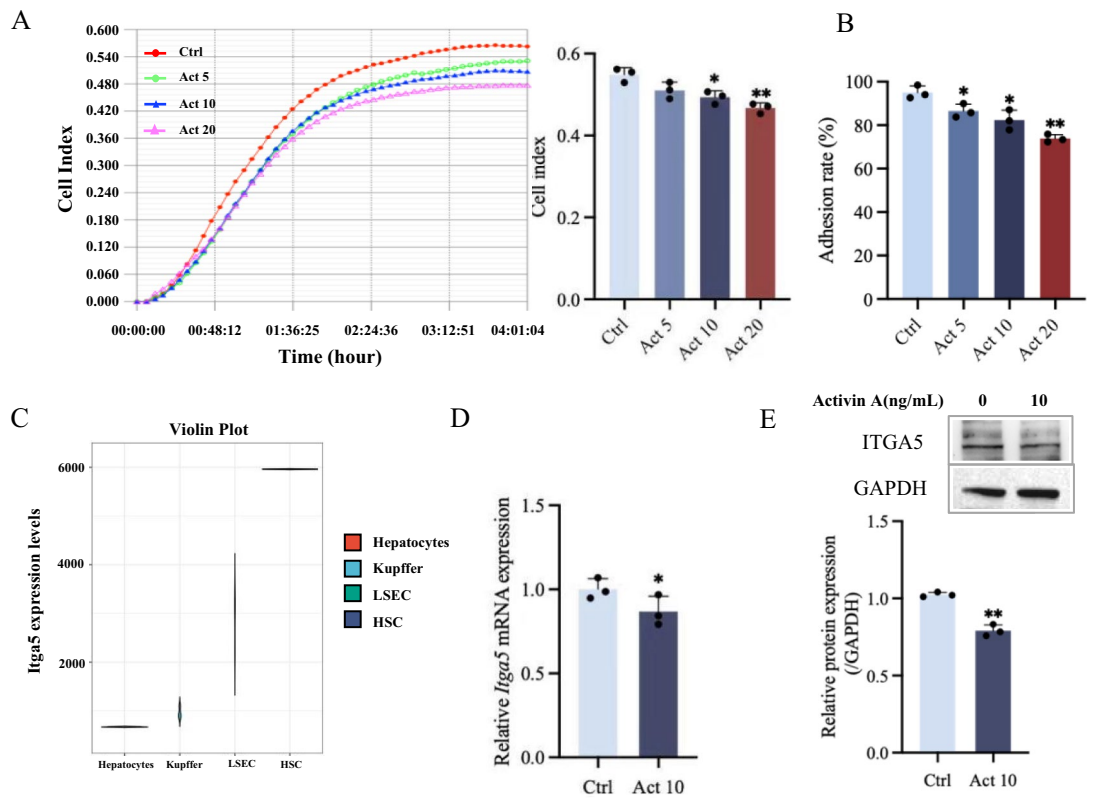


Fig. 4. Effect of activin A on MHStC adhesion. (A) Real-time cell adhesion was assessed through RTCA in the MHStCs treated with different activin A concentrations for 4 h. (B) Cell (96-well) culture plates were coated with 10 $\mu\text{g}/\text{mL}$ fibronectin and saturated with 1% BSA. MHStCs were seeded at a density of 2×10^4 cells/well. The adhered cells were measured using the CCK-8 kit. The number of MHStCs bound to the fibronectin-coated wells significantly decreased. (C) The violin plot showed *Itga5* gene expression in hepatocytes, Kupffer cells, LSECs, and HSCs. The *Itga5* mRNA and protein levels in the MHStCs treated with activin A (10 ng/mL) for 4 h were quantified by real-time PCR (D) and western blotting using GAPDH as the internal control protein (E). Ctrl, culture medium control. Act 5, 5 ng/mL activin A. Act 10, 10 ng/mL activin A. Act 20, 20 ng/mL activin A. * $P < 0.05$, ** $P < 0.01$ compared with the control group.

4 (ALK4) signaling molecules are novel regulators of EMT in human epicardial cells³⁸. Furthermore, activin A induces EMT and invasion in the ovarian and colon cancer cells^{39,40}. We, here, found that activin A-treated MHStCs exhibited MFB-like morphological changes, with an increase in the expression of N-cadherin, α -SMA, Vimentin, and MMP9 protein expressions. This suggested that the increase in activin A expression in liver injury can induce HSC activation, leading to the EMT process.

Integrins, the main cell adhesion receptors for components of the extracellular matrix (ECM), are a family of 24 transmembrane heterodimers, comprising 18 α integrin and 8 β integrin subunits⁴¹. Among integrin family members, integrin $\alpha 5$ (ITGA5) pairs with the $\beta 1$ subunit to form $\alpha 5\beta 1$ heterodimer. It plays a crucial role in governing cytoskeleton arrangement, cellular migration, apoptosis, and signaling by interacting with the ECM⁴². In addition, a study showed that macrophage-derived activin A induced enzalutamide resistance by upregulating a signaling cascade involving fibronectin—ITGA5 and tyrosine kinase Src⁴³. In the present study, activin A suppressed the expression levels of ITGA5 mRNA and protein, aligning with our observation that activin A hindered the adhesive ability of MHStCs to adhere to the ECM.

HSC migration is believed to be critical for HSC accumulation at the site of liver injury. For instance, CXCR3 expression on the HSCs activates Ras, Akt, and PI3-kinase pathways, thereby also promoting cell migration and proliferation⁴⁴. Numerous recent studies have suggested that activin A exerts regulatory effects on cell migration in several types of tumor and nontumor cells. Activin A selectively promotes in vitro directional migration of immature myeloid DCs (iDCs), which play a critical role in iDC recruitment to the inflammation sites⁴⁵. Exogenous activin A can promote colorectal cancer (CRC) cell migration, whereas knockdown of endogenous activin A exerts the opposite effects⁴⁶. Moreover, activin A downregulates E-cadherin expression by upregulating SLUG and SNAIL expressions through SMAD2/3-SMAD4-dependent signaling, which contributes to activin A-induced ovarian cancer cell migration. In our previous studies, activin A alone exhibited no effect on human neutrophil migration but inhibited human neutrophil migration toward fMLP chemotaxis and neutrophil recruitment to the localized skin infections in mice^{16,47}. Activin A also drives the chemotactic migration and adhesion of L929 fibroblasts through ERK signaling¹⁵. To investigate the effect of activin A on MHStC migration, we performed the scratch assay, transwell analysis, and microfluidic chip assay. Activin A was found to promote wound healing

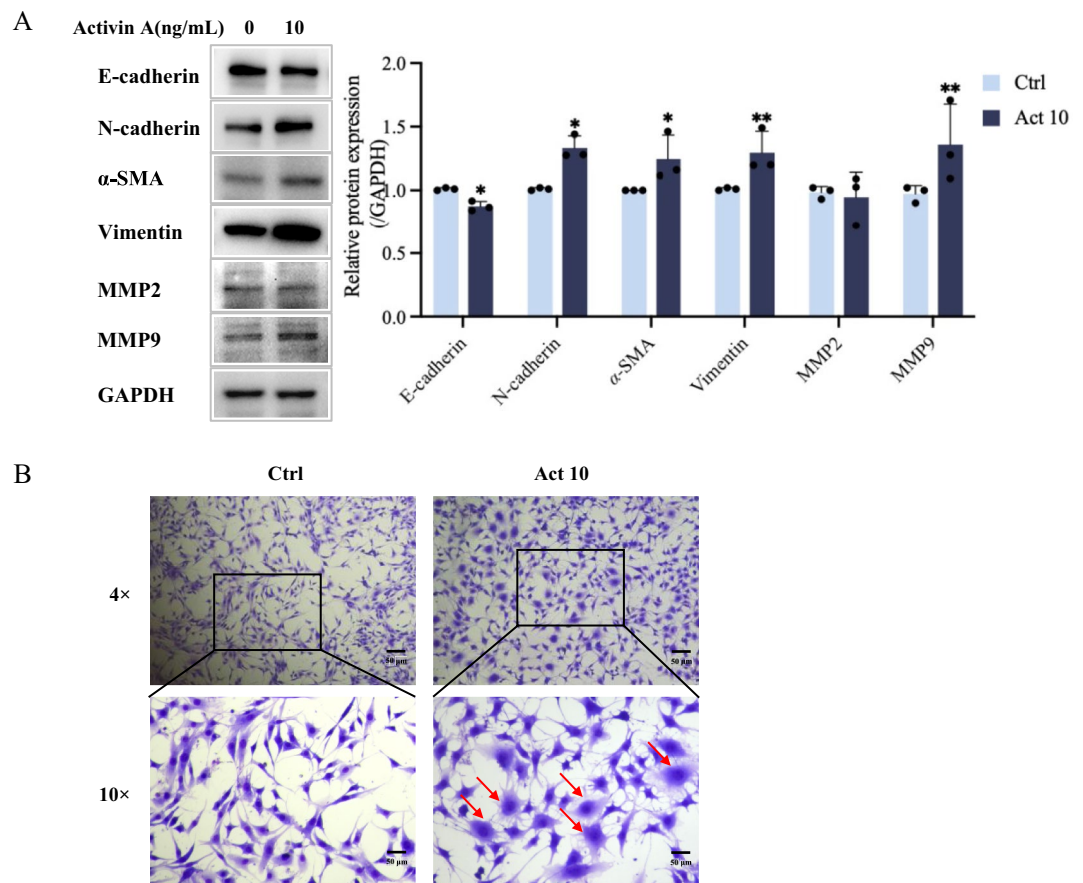


Fig. 5. Effect of activin A on the expression of migration-related proteins and morphology of MHSteCs. **(A)** The protein levels of E-cadherin, N-cadherin, α -SMA, Vimentin, MMP2, and MMP9 were determined by western blotting using GAPDH as the internal control protein. **(B)** The morphology of MHSteCs was examined following treatment with activin A (10 ng/mL) for 24 h. The red arrows indicate typical changes in cell morphology. Scale bar = 50 μ m. Ctrl, culture medium control. Act 10, 10 ng/mL activin A. * $P < 0.05$, ** $P < 0.01$ compared with the control group.

of the MHSteCs and increase the number of migrated cells as well as the distance of migration. These findings suggest that activin A, as a novel chemokine, can induce HSC migration.

The biological functions of activin A are facilitated by the participation of heteromeric receptor complexes comprising two distinct receptor types, namely type I and type II. Activin exhibits binding affinity toward activin receptor type 2A (ACVR2A) or activin receptor type 2B (ACVR2B), which then initiates the recruitment of a type I receptor, such as activin receptor type 1B (ACVR1B, also referred to as ALK4). The activated ACVR1B/ALK4 receptor then proceeds to recruit and phosphorylate SMAD2 and SMAD3, which then bind to the co-regulatory SMAD4, forming complexes for nuclear translocation where they regulate gene transcription. In addition to this Smad-dependent pathway, non-Smad pathways such as PI3K/AKT, MAPK/ERK, WNT/ β -catenin, and Notch pathways contribute to activin A signaling. The mechanism through which activin A exposure affects MHSteC migration, which was assessed in the present study, remains to be further elucidated; however, we can reasonably assume that activin A may affect the Smad pathway activation^{48–50}. Therefore, we next analyzed the protein expression of the classical Smad signaling pathway of activin. Activin A was found to significantly increase the p-Smad3 protein level and p-Smad3/Smad3 ratio in the MHSteCs, whereas no discernible alterations were observed in the levels of p-Akt and p-JNK, and the ratio of p-Akt/Akt and p-JNK/JNK. SIS3 is a potent and selective inhibitor of Smad3 function. As expected, SIS3 treatment significantly attenuated MHSteC migration and proliferation. These results suggest that activin A may regulate MHSteCs through the canonical Smad signaling pathway.

Calcium ions (Ca^{2+}) are recognized as second messengers and are crucial players in various cellular events, including transcription, endocytosis, intracellular membrane fusion, and cell migration²¹. Specifically, localized pulses of Ca^{2+} are predominantly observed at the leading edge of migrating cells. These pulses have been suggested to stimulate myosin activity, thereby facilitating nascent adhesions. Furthermore, these adhesions are presumed to serve as anchors for the traction generated by actin–myosin interaction, thereby supporting cell movement²¹. MICU1, a constituent of the mitochondrial calcium uniporter, acts as an ion channel complex that regulates the entry of calcium ions into mitochondria. In a study, the reduction in MICU1 levels led to excessive calcium accumulation within mitochondria²¹. Our previous studies have demonstrated that activin A has no

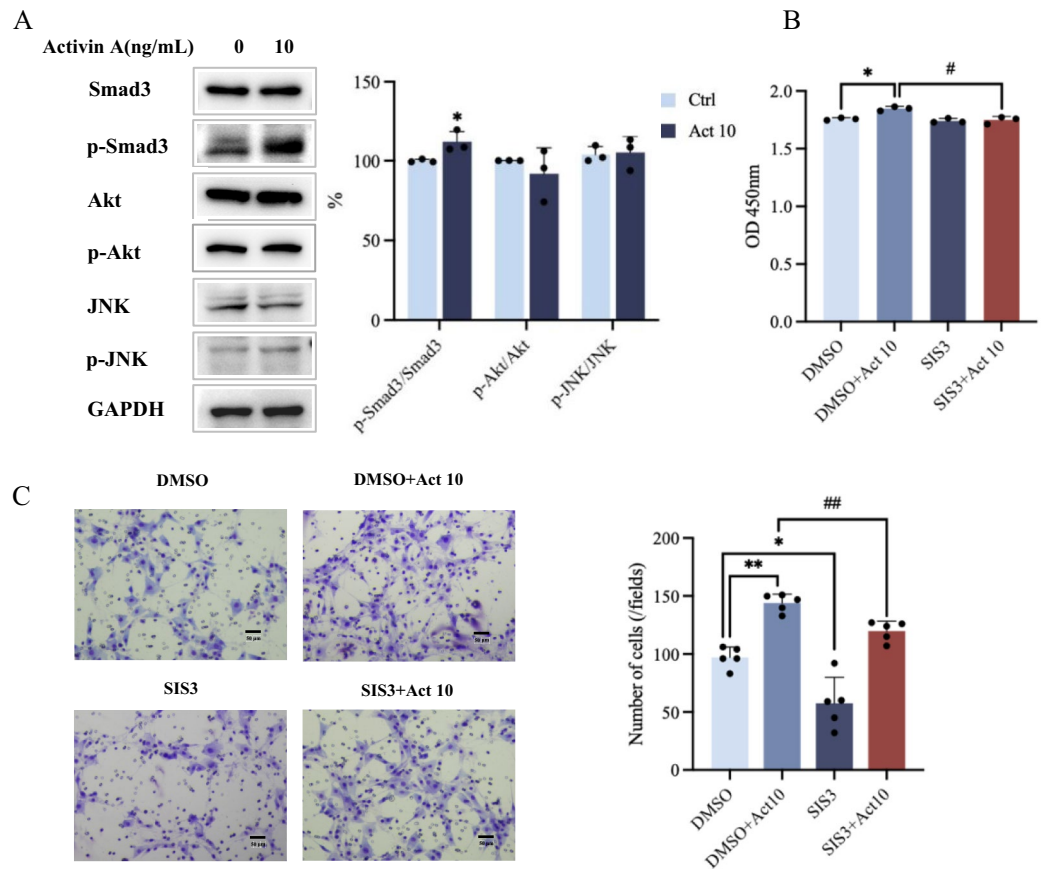


Fig. 6. Effect of activin A on the expression of Smad3 and non-Smad signaling proteins in MHSteCs. **(A)** The levels of Smad3 and p-Smad3, Akt and p-Akt, and JNK and p-JNK proteins were examined by western blotting, with GAPDH as the internal control protein. **(B)** MHSteCs were pretreated for 4 h with 0.025% DMSO or Smad3 inhibitor SIS3 (1 $\mu\text{mol/L}$) in 0.025% DMSO. Following the pretreatment, MHSteCs were exposed to 10 ng/mL activin A for 24 h. Then, the viability of MHSteCs was determined through the CCK-8 assay. **(C)** MHSteCs were pretreated for 4 h with 0.025% DMSO or 1 $\mu\text{mol/L}$ SIS3 in 0.025% DMSO. Then, MHSteC migration was determined through the transwell assay for 24 h ($n = 3$). Scale bar = 50 μm . Ctrl, culture medium as control group. DMSO, 0.025% DMSO as control group. SIS3, 1 $\mu\text{mol/L}$ SIS3 in 0.025% DMSO. Act 10, 10 ng/mL activin A. * $P < 0.05$, ** $P < 0.01$ compared with the control group. # $P < 0.05$, ## $P < 0.01$ compared with the DMSO + Act 10 group.

impact on the intracellular calcium flux in breast cancer cells¹⁶; however, it was found to stimulate fibroblast migration by increasing Ca^{2+} influx¹⁵. The present study demonstrated that activin A promoted Ca^{2+} influx in MHSteCs. Moreover, the stimulatory effect of activin A on MHSteC migration was effectively attenuated by BAPTA-AM. Additionally, activin A downregulated *Micu1* mRNA expression, further supporting the involvement of Ca^{2+} signaling in the migratory response of activin A-induced MHSteCs.

In conclusion, this study demonstrates that activin A inhibits mouse HSC adhesion and induces chemotactic migration of mouse HSCs by activating Smad3 and calcium signaling, offering a novel insight into the functional significance of activin A in the regulation of HSC activities in liver disease.

Material and methods

Cell lines and reagents

MHSteCs (ScienCell Research Laboratories, Carlsbad, CA, USA) were maintained in high-glucose DMEM supplemented with 10% fetal bovine serum (FBS) at 37°C in a humidified incubator containing 5% CO_2 . Cell counting kit-8 (CCK-8) was derived from GlpBio Biotechnology Co. (Montclair, CA, USA). Giemsa stain and dimethyl sulfoxide (DMSO) were purchased from Sigma-Aldrich (St. Louis, MO, USA). Recombinant human/mouse/rat activin A was obtained from R&D Systems (Minneapolis, MN, USA). Rat tail type I collagen was obtained from VWR international (Mississauga, Canada). Poly(dimethylsiloxane) (PDMS) pre-polymer (Sylgard 184) was purchased from Dow Corning (Midland, MI, USA). The mold for the microfluidic chip was a generous gift from Dr. Ke Yang, Hefei Institutes of Physical Science, CAS (Anhui, China).

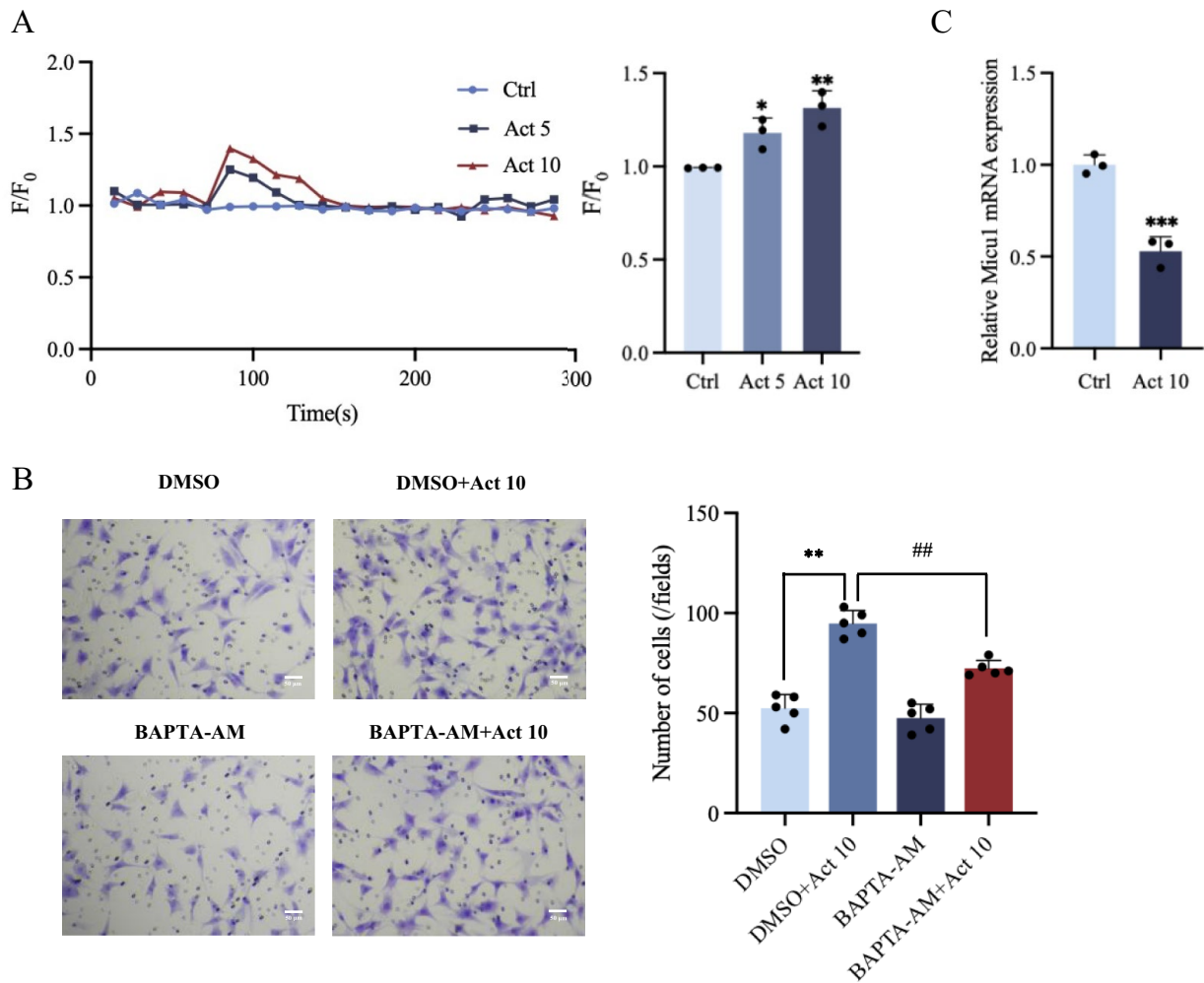


Fig. 7. Effect of activin A on calcium signaling in MHStCs. **(A)** MHStCs were incubated with the Ca²⁺-sensitive dye Fluo-4 (4 μ mol/L) for 40 min. The Fluo-4 signal was first recorded for 1 min to obtain the baseline fluorescence signal (F₀). The cells were then treated with activin A (5 and 10 ng/mL). The Fluo-4 signal of the simulated cells (F) was recorded for another 4 min. The experiment was repeated three times. The graph shows the peak values of the calcium signal upon stimulation with different activin A concentrations. The calcium level is represented by the Fluo-4 signal intensity normalized to the baseline (F/F₀). The graph represents the results from three separate experiments. **(B)** Effect of BAPTA-AM on cell migration in MHStCs. MHStCs were treated with 0.025% DMSO and 2.5 μ mol/L BAPTA-AM in 0.025% DMSO, and cell migration was determined through the transwell assay for 24 h. Scale bar = 50 μ m. **(C)** *Micu1* mRNA level was quantified through real-time PCR. Ctrl, culture medium as control group. DMSO, 0.025% DMSO as control group. BAPTA-AM, 2.5 μ mol/L BAPTA-AM in 0.025% DMSO. Act 5, 5 ng/mL activin A. Act 10, 10 ng/mL activin A. * P < 0.05, ** P < 0.01, *** P < 0.001 compared with the control group. ## P < 0.01 compared with the DMSO + Act 10 group.

Microarray data and identification of differentially expressed genes

The GSE226103 microarray dataset was downloaded from Gene Expression Omnibus (GEO, <http://www.ncbi.nlm.nih.gov/geo>). It comprises data of freshly isolated mouse hepatocytes, Kupffer cells, and LSECs, along with HSCs that have been cultured for 1, 7, or 14 days. We selected datasets of three hepatocyte samples (GSM7063818, GSM7063819, and GSM7063820) and two 1-day-cultured HSC samples (GSM7063827 and GSM7063828) as the objects. Subsequently, differential gene expression analysis was conducted using GEO2R (<http://www.ncbi.nlm.nih.gov/geo/geo2r/>). Volcano plots were analyzed using the online tool Hiplot (<https://hiplot.com.cn/>).

Cell proliferation assay

Cell proliferation was assessed using the CCK-8 assay. MHStCs were seeded at a density of 1×10^4 cells/well in a 96-well plate. Subsequently, the cells were incubated in 1% FBS-high-glucose DMEM supplemented with varying activin A concentrations (0, 5, 10, and 20 ng/mL) at 37°C under a 5% CO₂ atmosphere for 24, 48, and 72 h. Then, 10 μ L of the CCK-8 reagent was added to the culture medium (100 μ L) of each well, followed by the

incubation of the cells at 37°C for 2 h. Later, the absorbance was measured at 450 and 650 nm by using a micro-plate spectrophotometer. Each experiment was conducted in triplicate.

Extracellular matrix–cell adhesion assay

For extracellular matrix (ECM)–cell adhesion assays, 96-well plates were first coated with 10 µg/mL fibronectin and incubated at room temperature for 1 h, followed by saturation with PBS/1.0% bovine serum albumin (BSA) for 1 h at 37 °C. Then, the plates were washed twice with a serum-free medium. MHStECs (3.5×10^4 cells/well) were seeded onto the pre-coated 96-well plates and treated with 1% FBS-high glucose DMEM supplemented with varying activin A concentrations (0, 5, 10, and 20 ng/mL). The plates were then incubated at 37 °C for 2 h, and the cells were washed with PBS three times to remove non-adherent cells. One group of cells was left unwashed to determine the total cell count. Subsequently, the number of cells in each well was quantified using the CCK-8 method. The percentage of cell adhesion was calculated as follows: cell adhesion (%) = (adherent cell OD 450 value – blank OD 450 value)/(total cell OD 450 value – blank OD 450 value) × 100%. Each experiment was conducted in triplicate.

Wound healing assay

The wound scratch assay was performed to detect the wound healing ability of MHStECs. Briefly, the MHStECs were plated in 24-well culture plates. After the cells attached in the media containing 1% FBS, scratches were made by using a 100-µL plastic pipette tip. Floating cells were removed through gentle washing with PBS, and fresh media containing 1% FBS with or without activin A (5, 10 ng/mL) were added. Then, the cells were cultured in a 5% CO₂ incubator at 37 °C for 12 h. Scratch wound healing was observed and recorded using an inverted microscope. The scratch width was measured using Image J software for statistical analysis. Wound healing was expressed as the percentage of the original wound area that had healed.

Transwell chamber assay

Chemotactic migration of the MHStECs was evaluated through the transwell chamber assay as described previously¹⁵. In brief, 2×10^5 cells were seeded in the upper chambers (8-µm pore size; Corning, NY, USA) in 200 µL culture medium containing 1% FBS. The lower compartments were filled with 500 µL culture media supplemented with activin A (0, 5, and 10 ng/mL). Following 24-h incubation, the cells on the upper side of the chamber were eliminated using cotton-tipped swabs. The cells that had migrated through the insert membranes were fixed with 4% paraformaldehyde for 20 min and stained with Giemsa. The experiments were conducted in triplicate. The stained cells were visualized using the inverted microscope. The cell numbers were determined by counting the cells in five randomly selected fields from each chamber.

Microfluidic-based cell migration assay

The microfluidic D⁴-chip was used for examining MHStEC migration as described previously⁵². PDMS was mixed with a base in the 10:1 ratio, and the curing agent was degassed in the vacuum chamber. The PDMS was poured into the SU-8 master mold and cured at 80 °C for 2 h. The PDMS was peeled off the SU-8 mold. Its surface was treated using oxygen plasma (PDC-32G-2 Plasma System, 120 W, 500 mTorr, 20 s) and then bonded onto the substrate surface. Before the cells were inoculated into a microfluidic chip, 0.4% (w/v) BSA (Sigma-Aldrich, St Louis, MO, USA) was added to each chip for a 60-min incubation (37°C) and then removed. Subsequently, MHStECs were loaded from the cell loading inlets. The difference in pressure between the inlets and the other outlets caused the MHStECs to flow and be aligned beside the cell localization channels. Two groups of gradients, namely the medium–medium and medium–activin A (20 ng/mL), were generated in the D⁴-chip. In the medium–medium group, the medium was solely added, whereas in the medium–activin A group, both medium and activin A (20 ng/mL) were added to the medium–chemokine inlets at the same time, forming a stable chemical concentration gradient in the main channel of cell migration. The migration progress of the MHStECs was recorded using an inverted microscope. The capture frequency was set as 1 frame/4 h for 24 h to track cell trajectories in the same position. For chemotactic analysis, cell migration images were artificially tracked and analyzed using Image J software. Each experiment was performed in triplicate.

Real-time cell analysis

The RTCA instrument (xCELLigence RTCA S16; ACEA Biosciences, California, USA) was used to study the proliferation and adhesion properties of MHStECs. In the proliferation assay, 50 µL of 1% FBS-high glucose DMEM was added to the wells of the E16 xCELLigence microtiter plate, and the plate was then inserted into the RTCA device. After 1 min, the background impedance was measured for each well. Subsequently, MHStECs (1×10^4 cells in 100 µL of 1% FBS-high-glucose DMEM) were added to each well, cultured for 4 h, and treated with different activin A concentrations (0, 5, 10, and 20 ng/mL) for another 50 h.

In the adhesion assay, the E16 xCELLigence microtiter plates were initially coated with COL1 overnight at 4 °C, washed with PBS, and blocked with 1% BSA in PBS for 1 h at 37 °C. The wells were then washed with PBS once, and 50 µL of 1% FBS-high glucose DMEM was added to the wells of the E-plate 16. Cells and different concentrations of activin A were added together to each well. Adhesion curves were monitored for 4 h, with readings of the cell index (CI) taken every 15 min. The experiments were conducted in duplicate and repeated three times. The impedance of the cell sensor was characterized and quantified as the CI, which serves as an indicator of cell activity.

RT-PCR

Total RNA was extracted from MHStECs by using the RNAiso Plus reagent (Takara, Dalian, China), and reverse transcription was performed using the cDNA synthesis kit (CW BIO, CW2020M). PCR was conducted using 2× Es Taq MasterMix (CW BIO, CW0690H). The PCR conditions were as follows: an initial denaturation step at 95 °C for 1.5 min, followed by denaturation at 94 °C for 0.5 min, annealing at 56 °C for 0.5 min, and extension at 72 °C for 1 min, repeated for 30 cycles. A final extension step was performed at 72 °C for 10 min. Subsequently, PCR products were separated using 2% agarose gel electrophoresis and stained with Super Gelred (US EVER-BRIGHT, Suzhou, China). The PCR bands were visualized using ImageMaster VDS (Pharmacia Biotech; GE Healthcare) and digitized using Image J software. Table 1 presents the sequences of the primers used in this study.

Real-time quantitative PCR

SYBR Premix Ex Taq (Takara) was used for real-time quantitative PCR. The primers used were as follows: *Itga5*: 5'-GAAGCTCTGAAGATGCCCTACCA-3' (forward) and 5'-TGATGATCCACAACGGGACAC-3' (reverse); *Micu1*: 5'-ATCGAATCCGAGCCTACTC-3' (forward) and 5'-CTTCTCATTGGGCGTTATG-3' (reverse); and *GAPDH*: 5'-GCACCGTCAAGG CTGAGAAC-3' (forward) and 5'-TGGTGAAGACGCCAGTGGGA-3' (reverse). The reactions were performed using the Applied Biosystems QuantStudio3 FastReal-time PCR system (Thermo Fisher, USA). Quantified data were normalized to *GAPDH* data, and the relative quantity was calculated using the $2^{-\Delta\Delta CT}$ method.

Western blotting

MHStECs were lysed using a protein extraction reagent (Thermo Fisher Scientific, Waltham, MA, USA) supplemented with a cocktail of protease and phosphatase inhibitors (Thermo Fisher Scientific, USA) and 5 mmol/l EDTA solution. The proteins were quantified using a Pierce BCA protein assay kit (Thermo Fisher Scientific, USA) according to the manufacturer's instructions. Proteins (20 µg) were separated through 10% sodium dodecyl sulfate–polyacrylamide gel electrophoresis and transferred onto polyvinylidene difluoride membranes (Millipore, USA). For membrane blocking, the membranes were incubated with 5% skimmed milk in Tris-buffered saline with Tween-20 (TBS-T) at room temperature for 2 h with gentle shaking. After the membranes were blocked, they were incubated overnight at 4 °C with primary antibodies, followed by further incubation with the horseradish peroxidase-conjugated secondary antibody for 2 h at room temperature and enhanced chemiluminescent (ECL) detection (GE Healthcare, Little Chalfont, U.K.). Finally, the membranes were scanned using the LAS-4000 Luminescent Image Analyzer (Fujifilm, Japan). Experiments were conducted in three replicates. The immunoblots were quantified using Image J software, and the protein expression levels were normalized against those of *GAPDH*. Table 2 presents the antibodies used for western blotting.

Calcium flux assay

MHStECs were incubated with the Ca^{2+} -sensitive dye Fluo-4 (4 µmol/L) in dark for 40 min at 37 °C. The cells were washed with 1% FBS-high-glucose DMEM twice, and then, the Fluo-4 loaded cells were recovered in the incubator for 30 min in dark. The recovered cells were added to different tubes for analysis using a NovoCyte flow cytometer (NovoCyte, ACEA, USA). Initially, the baseline fluorescence signal (F_0) was obtained by recording the Fluo-4 signal for 1 min. After treating the cells with activin A (5 and 10 ng/mL), the Fluo-4 signal of the simulated cells (F) was recorded for another 4 min. FlowJo software (FlowJo LLC., Ashland, Oregon, US) was used to analyze the kinetics of Fluo-4 signal intensity. The calcium level is represented by the Fluo-4 signal intensity normalized to the baseline (F/F_0).

Gene	Primer	Sequence (5'-3')	Fragment size (bp)	Tm (°C)
<i>Gapdh</i>	F	GATTGTTGCCATCAACGACC	372	56
	R	GTGCAGGATGCATTGCTGAC		
<i>Inhba</i>	F	CGGGTATGTGGAGATAGAGGA	148	56
	R	CAGGTCCTGCCTTCCTTGGA		
<i>Smad2</i>	F	ATGGCCGTCTTCAGGTTTACACA	308	56
	R	ACTCTGTGGCTCAATTCCTGCT		
<i>Smad3</i>	F	CCAGCACACAATAACTTGGA	636	56
	R	AGACACACTGGAACAGCGGA		
<i>Acvr2a</i>	F	ATTGGCCAGCATCCATCTCTTG	294	56
	R	GCCACCATCATAGACTAGATTC		
<i>Acvr2b</i>	F	TGCTGAAGAGCGACCTCAC	544	56
	R	AGCAGGTCCACATTGGTGAC		
<i>Acvr1a</i>	F	GGTGTAAACAGGAACATCACGG	142	56
	R	GCAACTCCAAGGATGCAAGCT		

Table 1. Primer sequences for RT-PCR.

Antibodies	Source	Catalog number
Anti-GAPDH Rabbit pAb	Absin	Abs132004
Anti-Vimentin Rabbit mAb	Cell Signaling Technology	5741S
Anti-MMP2 Rabbit pAb	Abclonal	A6247
Anti-MMP9 Rabbit pAb	Proteintech	10,375-2-AP
Anti-N-cadherin Rabbit pAb	Proteintech	22,018-1-AP
Anti-E-cadherin Rabbit pAb	Proteintech	20,874-1-AP
Anti- α -SMA Rabbit mAb	Cell Signaling Technology	19245S
Anti-Integrin alpha 5 Rabbit pAb	Bioss	Bs-0567R
Anti-Akt Rabbit mAb	Cell Signaling Technology	4691S
Anti-Phospho-Akt Rabbit mAb	Cell Signaling Technology	4060S
Anti-JNK Rabbit pAb	Wanleibio	WL01295
Anti-Phospho-JNK Rabbit pAb	Wanleibio	WL01295
Anti-Smad3 Rabbit mAb	Abclonal	a22133
Anti-Phospho-Smad3-S423/S425 Rabbit pAb	Abclonal	ap1263

Table 2. Antibodies used for western blotting.

Statistical analysis

All data are expressed as the mean \pm standard deviation. Statistical analysis was performed using Student's *t*-test or a one-way ANOVA, followed by Tukey's multiple comparison test. The difference at $P < 0.05$ was considered statistically significant.

Data availability

Data is provided within the manuscript or supplementary information files.

Received: 24 February 2024; Accepted: 27 August 2024

Published online: 03 September 2024

References

- Bi, Y. *et al.* Polymorphisms in long noncoding RNA-prostate cancer-associated transcript 1 are associated with lung cancer susceptibility in a Northeastern Chinese population. *DNA Cell Biol.* **38**, 1357–1365. <https://doi.org/10.1089/dna.2019.4834> (2019).
- Lambrecht, J. *et al.* A PDGFR β -based score predicts significant liver fibrosis in patients with chronic alcohol abuse NAFLD and viral liver disease. *EBioMedicine* **43**, 501–512. <https://doi.org/10.1016/j.ebiom.2019.04.036> (2019).
- Seo, H. Y. *et al.* Evogliptin directly inhibits inflammatory and fibrotic signaling in isolated liver cells. *Int. J. Mol. Sci.* <https://doi.org/10.3390/ijms231911636> (2022).
- Sakamoto, K. *et al.* Heparin-binding epidermal growth factor-like growth factor and hepatocyte growth factor inhibit cholestatic liver injury in mice through different mechanisms. *Int. J. Mol. Med.* **38**, 1673–1682. <https://doi.org/10.3892/ijmm.2016.2784> (2016).
- Zuo, L. *et al.* PI3-kinase/Akt pathway-regulated membrane transportation of acid-sensing ion channel 1a/Calcium ion influx/endoplasmic reticulum stress activation on PDGF-induced HSC Activation. *J. Cell Mol. Med.* **23**, 3940–3950. <https://doi.org/10.1111/jcmm.14275> (2019).
- Kiagiadaki, F. *et al.* Activin-A causes Hepatic stellate cell activation via the induction of TNF α and TGF β in Kupffer cells. *Biochim. Biophys. Acta Mol. Basis Dis.* **891**–899, 2018. <https://doi.org/10.1016/j.bbdis.2017.12.031> (1864).
- Refaat, B. *et al.* Profiling activins and follistatin in colorectal cancer according to clinical stage, tumour sidedness and Smad4 status. *Pathol. Oncol. Res.* **27**, 1610032. <https://doi.org/10.3389/pore.2021.1610032> (2021).
- Whiley, P. A. F., Nathaniel, B., Stanton, P. G., Hobbs, R. M. & Loveland, K. L. Spermatogonial fate in mice with increased activin A bioactivity and testicular somatic cell tumours. *Front. Cell Dev. Biol.* **11**, 1237273. <https://doi.org/10.3389/fcell.2023.1237273> (2023).
- Chen, C. W. *et al.* Activin A downregulates the CD69-MT2A axis via p38MAPK to induce erythroid differentiation that sensitizes BCR-ABL-positive cells to imatinib. *Exp. Cell Res.* **417**, 113219. <https://doi.org/10.1016/j.yexcr.2022.113219> (2022).
- Liu, H. *et al.* Beneficial effects of moderate hepatic activin A expression on metabolic pathways, inflammation, and atherosclerosis. *Arterioscler. Thromb. Vasc. Biol.* **43**, 330–349. <https://doi.org/10.1161/atvbaha.122.318138> (2023).
- Taniguchi, S. *et al.* In vivo induction of activin A-producing alveolar macrophages supports the progression of lung cell carcinoma. *Nat. Commun.* **14**, 143. <https://doi.org/10.1038/s41467-022-35701-8> (2023).
- Pinjusic, K. *et al.* Activin-A impairs CD8 T cell-mediated immunity and immune checkpoint therapy response in melanoma. *J. Immunother. Cancer* **10**, e004533. <https://doi.org/10.1136/jitc-2022-004533> (2022).
- Patella, S., Phillips, D. J., Tchongue, J., de Kretser, D. M. & Sievert, W. Follistatin attenuates early liver fibrosis: Effects on hepatic stellate cell activation and hepatocyte apoptosis. *Am. J. Physiol. Gastrointest. Liver Physiol.* **290**, G137–144. <https://doi.org/10.1152/ajpgi.00080.2005> (2006).
- Friedman, S. L. Hepatic stellate cells: Protean, multifunctional, and enigmatic cells of the liver. *Physiol. Rev.* **88**, 125–172. <https://doi.org/10.1152/physrev.00013.2007> (2008).
- Jiang, L. *et al.* Activin A as a novel chemokine induces migration of L929 fibroblasts by ERK signaling in microfluidic devices. *Front. Cell Dev. Biol.* **9**, 660316. <https://doi.org/10.3389/fcell.2021.660316> (2021).
- Xie, D. *et al.* The effects of activin A on the migration of human breast cancer cells and neutrophils and their migratory interaction. *Exp. Cell Res.* **357**, 107–115. <https://doi.org/10.1016/j.yexcr.2017.05.003> (2017).
- Otaka, A. *et al.* Quantification of cell co-migration occurrences during cell aggregation on fibroin substrates. *Tissue Eng. Part C Methods* **20**, 671–680. <https://doi.org/10.1089/ten.TEC.2013.0344> (2014).
- Wang, W. *et al.* NLRC5 modulates bone metabolism and plays a role in periodontitis. *J. Periodontol. Res.* **57**, 891–903. <https://doi.org/10.1111/jre.13027> (2022).

19. Rezechova, I. *et al.* Type 3 inositol 1,4,5-trisphosphate receptor has antiapoptotic and proliferative role in cancer cells. *Cell Death Dis.* **10**, 186. <https://doi.org/10.1038/s41419-019-1433-4> (2019).
20. Li, L. *et al.* Long noncoding RNA RMRP contributes to paclitaxel sensitivity of ovarian cancer by regulating miR-580-3p/MICU1 signaling. *J. Oncol.* **2022**, 8301941. <https://doi.org/10.1155/2022/8301941> (2022).
21. Dong, Z. *et al.* Exosomal miR-181a-2-3p derived from citreoviridin-treated hepatocytes activates hepatic stellate cells through inducing mitochondrial calcium overload. *Chem. Biol. Interact.* **358**, 109899. <https://doi.org/10.1016/j.cbi.2022.109899> (2022).
22. Liu, T. *et al.* The CYP2E1 inhibitor DDC up-regulates MMP-1 expression in hepatic stellate cells via an ERK1/2- and Akt-dependent mechanism. *Biosci. Rep.* **33**, e00041. <https://doi.org/10.1042/bsr20130033> (2013).
23. Liu, Z. *et al.* XBP1 deficiency promotes hepatocyte pyroptosis by impairing mitophagy to activate mtDNA-cGAS-STING signaling in macrophages during acute liver injury. *Redox Biol.* **52**, 102305. <https://doi.org/10.1016/j.redox.2022.102305> (2022).
24. Hardy, C. L. *et al.* The activin A antagonist follistatin inhibits cystic fibrosis-like lung inflammation and pathology. *Immunol. Cell Biol.* **93**, 567–574. <https://doi.org/10.1038/icb.2015.7> (2015).
25. Manavski, Y. *et al.* Endothelial transcription factor KLF2 negatively regulates liver regeneration via induction of activin A. *Proc. Natl. Acad. Sci. USA* **114**, 3993–3998. <https://doi.org/10.1073/pnas.1613392114> (2017).
26. Bian, X. *et al.* Senescence marker activin A is increased in human diabetic kidney disease: Association with kidney function and potential implications for therapy. *BMJ Open Diabetes Res. Care* **7**, e000720. <https://doi.org/10.1136/bmjdr-2019-000720> (2019).
27. Peng, W. *et al.* Activin A and CCR2 regulate macrophage function in testicular fibrosis caused by experimental autoimmune orchitis. *Cell Mol. Life Sci.* **79**, 602. <https://doi.org/10.1007/s00018-022-04632-4> (2022).
28. Hu, J. *et al.* Activin A stimulates the proliferation and differentiation of cardiac fibroblasts via the ERK1/2 and p38-MAPK pathways. *Eur. J. Pharmacol.* **789**, 319–327. <https://doi.org/10.1016/j.ejphar.2016.07.053> (2016).
29. Andreev, K. *et al.* Expression of bone morphogenetic proteins (BMPs), their receptors, and activins in normal and scarred conjunctiva: Role of BMP-6 and activin-A in conjunctival scarring? *Exp. Eye Res.* **83**, 1162–1170. <https://doi.org/10.1016/j.exer.2006.06.003> (2006).
30. Ly, T. D. *et al.* Activin A-mediated regulation of XT-I in human skin fibroblasts. *Biomolecules* **10**, 609. <https://doi.org/10.3390/biom10040609> (2020).
31. Chen, Y. I. *et al.* Homophilic ATP1A1 binding induces activin A secretion to promote EMT of tumor cells and myofibroblast activation. *Nat. Commun.* **13**, 2945. <https://doi.org/10.1038/s41467-022-30638-4> (2022).
32. Wei, Q. *et al.* The expression and role of activin A and follistatin in heart failure rats after myocardial infarction. *Int. J. Cardiol.* **168**, 2994–2997. <https://doi.org/10.1016/j.ijcard.2013.04.012> (2013).
33. Wang, D. H. *et al.* Role of activin A in carbon tetrachloride-induced acute liver injury. *World J. Gastroenterol.* **19**, 3802–3809. <https://doi.org/10.3748/wjg.v19.i24.3802> (2013).
34. Yu, S. Y. *et al.* Uncovering tumor-promoting roles of activin A in pancreatic ductal adenocarcinoma. *Adv. Sci. (Weinh)* **10**, e2207010. <https://doi.org/10.1002/advs.202207010> (2023).
35. Li, Y. *et al.* Activin A secreted from peripheral nerve fibroblasts promotes proliferation and migration of schwann cells. *Front. Mol. Neurosci.* **15**, 859349. <https://doi.org/10.3389/fnmol.2022.859349> (2022).
36. Wiley, M. B. *et al.* Non-canonical activin A signaling stimulates context-dependent and cellular-specific outcomes in CRC to promote tumor cell migration and immune tolerance. *Cancers* **15**, 3003. <https://doi.org/10.3390/cancers15113003> (2023).
37. Yu, F., Geng, W., Dong, P., Huang, Z. & Zheng, J. LncRNA-MEG3 inhibits activation of hepatic stellate cells through SMO protein and miR-212. *Cell Death Dis.* **9**, 1014. <https://doi.org/10.1038/s41419-018-1068-x> (2018).
38. Dronkers, E. *et al.* Activin A and ALK4 identified as novel regulators of epithelial to mesenchymal transition (EMT) in human epicardial cells. *Front. Cell Dev. Biol.* **9**, 765007. <https://doi.org/10.3389/fcell.2021.765007> (2021).
39. Basu, M. *et al.* Invasion of ovarian cancer cells is induced by PITX2-mediated activation of TGF- β and Activin-A. *Mol. Cancer* **14**, 162. <https://doi.org/10.1186/s12943-015-0433-y> (2015).
40. Bauer, J. *et al.* Increased stiffness of the tumor microenvironment in colon cancer stimulates cancer associated fibroblast-mediated prometastatic activin A signaling. *Sci. Rep.* **10**, 50. <https://doi.org/10.1038/s41598-019-55687-6> (2020).
41. Hamidi, H. & Ivaska, J. Every step of the way: integrins in cancer progression and metastasis. *Nat. Rev. Cancer* **18**, 533–548. <https://doi.org/10.1038/s41568-018-0038-z> (2018).
42. Zhao, D. *et al.* Osteocytes regulate bone anabolic response to mechanical loading in male mice via activation of integrin $\alpha 5$. *Bone Res.* **10**, 49. <https://doi.org/10.1038/s41413-022-00222-z> (2022).
43. Li, X. F. *et al.* Macrophages promote anti-androgen resistance in prostate cancer bone disease. *J. Exp. Med.* **220**, e20221007. <https://doi.org/10.1084/jem.20221007> (2023).
44. Khodayari, N. *et al.* Alpha-1 antitrypsin deficient individuals have circulating extracellular vesicles with profibrogenic cargo. *Cell Commun. Signal* **18**, 140. <https://doi.org/10.1186/s12964-020-00648-0> (2020).
45. Salogni, L. *et al.* Activin A induces dendritic cell migration through the polarized release of CXC chemokine ligands 12 and 14. *Blood* **113**, 5848–5856. <https://doi.org/10.1182/blood-2008-12-194597> (2009).
46. Daitoku, N. *et al.* Activin A promotes cell proliferation, invasion and migration and predicts poor prognosis in patients with colorectal cancer. *Oncol. Rep.* **47**, 1–9. <https://doi.org/10.3892/or.2022.8318> (2022).
47. Qi, Y. *et al.* Activin A impairs ActRIIA(+) neutrophil recruitment into infected skin of mice. *iScience* **24**, 102080. <https://doi.org/10.1016/j.isci.2021.102080> (2021).
48. Groppe, J. C. *et al.* Polypeptide substrate accessibility hypothesis: gain-of-function R206H mutation allosterically affects activin receptor-like protein kinase activity. *Biomolecules* **13**, 1129. <https://doi.org/10.3390/biom13071129> (2023).
49. Cui, X. *et al.* Perspectives of small molecule inhibitors of activin receptor-like kinase in anti-tumor treatment and stem cell differentiation (Review). *Mol. Med. Rep.* **19**, 5053–5062. <https://doi.org/10.3892/mmr.2019.10209> (2019).
50. Bloise, E. *et al.* Activin A in mammalian physiology. *Physiol. Rev.* **99**, 739–780. <https://doi.org/10.1152/physrev.00002.2018> (2019).
51. Hammad, A. S. & Machaca, K. Store operated calcium entry in cell migration and cancer metastasis. *Cells* **10**, 1246. <https://doi.org/10.3390/cells10051246> (2021).
52. Liu, G. *et al.* Follistatin is a crucial chemoattractant for mouse decidualized endometrial stromal cell migration by JNK signalling. *J. Cell Mol. Med.* **27**, 127–140. <https://doi.org/10.1111/jcmm.17648> (2023).

Acknowledgements

This work was supported by the Foundation of Science and Technology Department of Jilin Province (20220402079GH and 20240404027ZP), China.

Author contributions

Conceptualization: X.C. and Y.L.; methodology: K.Y. and W.Z.; software: F.Z. and R.W.; validation: W.Z., L.Z. and F.F.; formal analysis: W.Z. and L.Z.; investigation: W.Z., X.C. and L.Z.; resources: X.C. and Y.L.; data curation: W.Z.; writing—original draft, W.Z. and X.C.; writing—review and editing: W.Z., Y.L. and X.C.; visualization: W.Z. and K.Y.; supervision: X.C.; project administration: Y.L.; funding acquisition: X.C. All authors have read and agreed to the published version of the manuscript.

Competing interests

The authors declare no competing interests.

Additional information

Supplementary Information The online version contains supplementary material available at <https://doi.org/10.1038/s41598-024-71304-7>.

Correspondence and requests for materials should be addressed to Y.L. or X.C.

Reprints and permissions information is available at www.nature.com/reprints.

Publisher's note Springer Nature remains neutral with regard to jurisdictional claims in published maps and institutional affiliations.

Open Access This article is licensed under a Creative Commons Attribution-NonCommercial-NoDerivatives 4.0 International License, which permits any non-commercial use, sharing, distribution and reproduction in any medium or format, as long as you give appropriate credit to the original author(s) and the source, provide a link to the Creative Commons licence, and indicate if you modified the licensed material. You do not have permission under this licence to share adapted material derived from this article or parts of it. The images or other third party material in this article are included in the article's Creative Commons licence, unless indicated otherwise in a credit line to the material. If material is not included in the article's Creative Commons licence and your intended use is not permitted by statutory regulation or exceeds the permitted use, you will need to obtain permission directly from the copyright holder. To view a copy of this licence, visit <http://creativecommons.org/licenses/by-nc-nd/4.0/>.

© The Author(s) 2024